AlGaAs-GaAs CASCADE SOLAR CELL*

M. F. Lamorte and D. H. Abbott
Research Triangle Institute
Research Triangle Park, North Carolina

ABSTRACT

Computer modeling studies are reported for a monolithic, two-junction, cascade solar cell using the AlGaAs-GaAs materials combination. An optimum design is obtained through a serial optimization procedure by which conversion efficiency is maximized for operation at 300 K, AM 0, and unity solar concentration. Under these conditions the upper limit on efficiency is shown to be in excess of 29%, provided surface recombination velocity does not exceed 10^4cm sec^{-1}.

INTRODUCTION

Computer modeling shows that conversion efficiency exceeding 30% may be realized from a two-junction cascade solar cell at 300 K and AM 0 [ref. 1-5]. These investigations show that the bandgap of the wide (top) and narrow (bottom) bandgap cells more strongly influence the efficiency than other design parameters. While steady progress has been made in the development of the technology required to obtain high efficiency, the technological problems encountered in this endeavor has generally limited the efficiency to 15% or less [ref. 6,7]. The major problem is the difficulty of fabricating a structure with an optimum bandgap combination because of lattice mismatch [ref. 4]. Related problems spring from the adverse effects arising from short diffusion length, control of layer thickness, space charge recombination current, p-n junction leakage current, and fabrication of a large area, low voltage drop tunnel junction.

The optimum bandgap combinations range from 1.62 eV/0.95 eV [ref. 1-4] to 1.84 eV/1.23 eV [ref. 5] where the efficiency is maximized at 300 K at AM 0 and 475 K at AM 1, respectively, using the AlGaAs-GaInAs materials combination. While the lattice mismatch is reduced with increasing bandgap values in this material system, cascade cells have not been fabricated with high efficiency using these bandgap combinations because of poor crystalline quality due to large lattice mismatch. However, one encouraging factor is that the upper limit efficiency for the 1.84 eV/1.23 eV [ref. 5] set at AM 1 is approximately 30% which is only slightly lower than the 31.5% obtained for the optimum combination 1.62 eV/0.95 eV [ref. 1-4] at 300 K and AM 0. If further compromise is made with respect to efficiency, a range of bandgap values may exist which are higher than the 1.84 eV/1.23 eV combination that give 25% or higher efficiency values for optimized designs [ref. 4]. The attractiveness of these considera-

*This work was supported by the Air Force Aeronautical Laboratory, Wright-Patterson Air Force Base, Dayton, OH, Contract No. F33615-78-C-2077.

tions is that further increases in bandgap continues to decrease the lattice mismatch, where at the extreme the AlGaAs-GaAs materials combination shows a very small lattice mismatch over its entire compositional range [ref. 4]. Although the electronic and optical properties of AlGaAs have not been studied as extensively as for GaAs, there is a sufficient body of experimental data to suggest that the properties of AlGaAs are favorable for the fabrication of cascade cells [ref. 8,9].

The major obstacle to the fabrication of high efficiency cells using the AlGaAs materials system is that its bandgap span does not encompass the optimum bandgap combinations which give efficiency values of 30% or greater [ref. 4]. Initial studies indicated that a non-optimized design may give cascade efficiency values less than 15% [ref. 4]. The efficiency which may be attainable for an optimized design has not been studied. Other problems such as the fabrication of a low voltage drop tunnel junction and low resistance ohmic contact to AlGaAs appear to be solved or nearing solution [ref. 10,11]. On balance, the seriousness with which this materials combination is to be considered in cascade cell fabrication depends heavily on the device design requirements and the corresponding upper limit on efficiency. In this paper computer modeling results are reported with presentation of an optimum design and its corresponding maximum efficiency for operation at 300 K, AM 0, and unity solar concentration.

The computer modeling program is applied to the bandstructure shown in figure 1 [ref. 1-5]. Top and bottom cells are joined electrically through a tunnel junction, and with the window layer form a monolithic structure. The cascade photovoltage is the sum of the top and bottom photovoltages which are of the same polarity. In this connection, it is essential that the tunnel junction should not absorb photons [ref. 1-5]. Should this occur, the photon flux available to the bottom cell is reduced and the resultant photovoltage generated in the tunnel junction subtracts from the sum of the top and bottom cell photovoltages. Also, this may produce a mismatch in the currents at the maximum power point of the individual V-I curves of top and bottom cells. All of these effects serve to reduce cascade efficiency.

The bottom cell is assigned the value 1.44 eV, corresponding to the GaAs bandgap, because it is the minimum value which is obtainable from the AlGaAs-GaAs materials combination. Therefore, the optimum bandgaps of the top cell and window layer are required to be obtained from the optimization procedure [ref. 1-5]. Typically, setting the tunnel junction bandgap equal to the top cell bandgap produces an optimum design, while minimizing the technological difficulties. Also, the window layer thickness typically used is 0.1 μm, with $2 \times 10^{18} cm^{-3}$ acceptor concentration, and a linear bandgap grading to establish a 3000 V cm^{-1} built-in potential [ref. 1-5].

In the present fabrication process involving liquid phase epitaxy, the acceptor concentration in the p-type regions of top and bottom cells is $10^{18} cm^{-3}$ and cannot easily be changed [ref. 12]. Therefore, optimized acceptor concentrations are not determined for these regions. The tunnel junction donor concentration is set at $10^{19} cm^{-3}$, acceptor concentration at $10^{20} cm^{-3}$, and 0.1 μm thickness for the n- and p-regions. Optimized donor and acceptor concentrations and layer thicknesses are determined for all other regions.

The analytical method developed for cascade solar cells has been described elsewhere and is not discussed in detail in this paper [ref. 1,2,4]. By formulating the solution of the continuity equations in the framework of a boundary value problem, the cascade cell V-I relationship may be obtained, in principle, in closed form. However, in the simplest of cases solving for the current requires the solution of 14 simultaneous equations, for which the inversion is performed using a digital computer and the closed form equation is never explicitly obtained.

The other assumptions used in the analysis are that the thermal diffusion contribution to dark current is large compared to space-charge recombination and excess tunnel current components; the minority-carrier recombination rate is linearly proportional to excess carrier concentration [ref. 9,13]; recombination at heterojunction interfaces are negligible; efficiency is not corrected for grid contact shadowing or for power loss from joule heating arising in the structure's series resistance; and reflectivity at the window surface is 5%.

Device performance characteristics and parameters used in the study, for the most part, are those which have become standard in the photovoltaic literature. However, in cascade solar cells a number of additional parameters are needed to more completely characterize the device. They are usually defined in the discussion. In our studies the normalized collection efficiency is used exclusively, and is defined as the ratio of carriers collected by the p-n junction to the carriers generated through photon absorption in the region under consideration.

In the optimization study reported here, the invariant operating conditions imposed in all calculations are AM 0, unity solar concentration, and $10^6 cm \cdot s^{-1}$ surface recombination velocity.

COMPUTER MODELING RESULTS

In this section the computer modeling results are presented and discussed. Investigation is devoted to the determination of an optimized cascade cell design. Analysis of the device performance characteristics of this optimized structure, shows that the surface recombination loss may be the major loss factor in the AlGaAs-GaAs cascade cell.

Various optimization procedures may be used. The more desirable procedure is to allow all parameters to simultaneously vary over a specific range of values, which results in the determination of the optimum value for each parameter. Computer costs are usually prohibitive and this method is almost never used. The other extreme is a serial optimization that is used in this study. Computer costs in this case are typically low, but it usually requires greater skill in establishing the range of values for each of the parameters to avoid obtaining false optimum values [ref. 1,2,4]. In the serialization procedure used here the optimum value of one parameter is obtained by allowing only that parameter to vary over a judiciously selected range and determining the value for which the efficiency is a maximum. The values of the other parameters are held constant at values which are determined, by other considerations, to be in

the neighborhood of their optimum values. The optimum value of the one parameter so determined is then imposed on the structure. A second parameter is then allowed to vary and its optimum value determined and also imposed on the structure. This procedure is repeated for each parameter in a selected sequence. After having determined the optimum value for each parameter, the procedure is repeated a second time for each parameter in the same sequence. Typically, the same optimum values are obtained, while in some cases there are corrections for one or more of the parameter values. If the corrections are significant, the procedure is repeated for each of the parameters until the same optimum values are obtained. In the serial optimization used here, the optimum values of the parameters of the top cell are determined first, and then those of the bottom cell. Thus, in this sequence the performance characteristics of the top cell are unaffected when the bottom cell parameters are permitted to vary. However, when the bottom cell parameters are permitted to vary the current mismatch between top and bottom cells is affected.

Serial Optimization Results

The computer modeling results presented below are those obtained for the second serialization. The optimum values obtained from the second serialization are not significantly different from those obtained from the first set of optimum values, therefore, a third serialization procedure is not necessary.

Figures 2(a) to 2(d) show the effects when the top cell bandgap is allowed to vary in the range 1.88 eV to 1.98 eV, while all other parameters are held constant as given in figure 1. Maximum efficiency is 27.6% which occurs at 1.94 eV in figure 1(a). This is considerably lower than the 31.5% value obtained in the more favorable cascade cell using AlGaAs-GaInAs where the optimum top cell bandgap is 1.62 eV.

A figure-of-merit which is useful in describing cascade cell operation is the excess current of the top cell defined by

$$\Delta J_{exT} = J_{mp} - J_{mpT} \tag{1}$$

and for the bottom cell by

$$\Delta J_{exB} = J_{mp} - J_{mpB} \quad , \tag{2}$$

where J_{mp}, J_{mpT}, J_{mpB} represent the current densities at the maximum power point of the cascade V-I curve, and of the independently operated V-I curves of top and bottom cells, respectively. The excess current parameters, exhibited in figure 2(b), are a measure of the power which is not delivered to the cascade cell terminals and which, as a result, is dissipated internally. In our studies, the values of ΔJ_{exT} and ΔJ_{exB} are typically less than 0.1 $mAcm^{-2}$ for an optimized design.

Reduction of the excess current of the top and bottom cells results in increasing the current, J_{mp}, at the maximum power point on the cascade cell V-I curve. This is shown in figure 2(c) where J_{mp} increases for increasing E_{GT} values above 1.88 eV, attains a pronounced maximum at 1.94 eV, and is reduced for bandgap values above 1.94 eV. Thus, it is seen that the maximum value, 15.8 $mAcm^{-2}$, occurs at the same E_{GT} value as for maximum efficiency.

In figure 2(d) is shown the power utilization factor P_u vs E_{GT}, which is defined by the relationship

$$P_u = \frac{P_{mpc}}{P_{mpT} + P_{mpB}} \quad , \tag{3}$$

where P_{mpc}, P_{mpT}, and P_{mpB} are the power at the maximum power point of the cascade, top, and bottom cell V-I curves, respectively. The ratio in equation (3) is typically less than 0.98, and contains only losses due to current mismatch, and tunnel junction joule power loss. It is independent of optical, recombination, and dark current loss contributions. P_u also increases to a sharp peak at 1.94 eV and falls off quite rapidly on either side of its maximum.

Region 3 donor concentration is the second parameter selected in the sequence of parameter optimization in the determination of an optimized design. The range chosen for the concentration is $5 \times 10^{16} cm^{-3}$ to $8 \times 10^{18} cm^{-3}$, all other parameters held constant using the values given in figure 1. Maximum efficiency is shown to occur in figure 3(a) at $8 \times 10^{17} cm^{-3}$. While the slope is small for concentration values less than $8 \times 10^{17} cm^{-3}$, it is strongly negative for higher values. Figure 3(b) describes the monotonic decrease of the hole normalized collection efficiency which results because of the monotonic decrease of the hole diffusion length with increasing concentration. Both parameters decrease gradually with increasing concentration up to $3 \times 10^{18} cm^{-3}$ and for higher values they decrease sharply. Thus, the rapid decrease in conversion efficiency above $3 \times 10^{18} cm^{-3}$ has its source in the rapid decrease in the hole diffusion length. This occurs because the model contains the effects of the rapid decrease in hole lifetime and mobility in Region 3 in the concentration range above $3 \times 10^{18} cm^{-3}$.

The hole dark current coefficient is also strongly influenced by the donor concentration as shown in figure 3(c). The hole dark current coefficient decreases inversely with donor concentration whereas the electron dark current coefficient is constant. The decrease is rapid up to $3 \times 10^{18} cm^{-3}$, becoming less rapid for higher concentration values. The latter results because of an opposing trend in which the rapid decrease in hole diffusion length tends to increase the hole contribution to dark current. Consequently the total dark current coefficient, the sum of the hole and electron components, decreases rapidly up to a concentration of $8 \times 10^{17} cm^{-3}$ where the electron and hole contributions approach equality and then levels off as the invariant electron component comes to dominate the sum. This saturation effect is reflected in the behavior of the voltage at the maximum power point which is also shown. Thus it is seen that the balancing of the dark current coefficient components determines the optimum value of donor concentration. If the rapid decrease in collection efficiency

had occurred at a concentration lower than 8 x $10^{18}cm^{-3}$ then the situation would have been reversed. The breakpoint in collection efficiency slope rather than the breakpoint in dark current coefficient slope would have determined the optimum value of donor concentration.

Maximum power available from the top cell, P_{mpT}, to the cascade unit, shown in figure 3(d), increases gradually up to 8 x $10^{17}cm^{-3}$ and then shows a rapid decrease for higher concentrations, which is attributed to the behavior of the hole collection efficiency in this range. Also shown, the power utilization ratio is constant up to 2 x $10^{18}cm^{-3}$ and then decreases for higher concentration values. This decrease arises because the decrease in hole collection efficiency produces an increasing current mismatch between top and bottom cells.

In determining the optimum thickness of Regions 2 and 3 a two-step procedure is employed. The first step is to obtain the optimum value of the ratio $(X_2-X_1)/(X_3-X_1)_{opt}$, denoted p-ratio, and the second to obtain the optimum value of the ratio $(X_3-X_1)/X_3-X_1)_{opt}$, where $(X_3-X_1)_{opt}$ is the optimum value of the sum of the p- and n- region thicknesses. Subsequently, it is shown that the value of $(X_3-X_1)_{opt}$ = 1.46 μm.

Maximum efficiency is 27.6% in figure 4(a), occurring at the value 0.3 for the p-ratio. It is seen not to exhibit a strong dependency on the p-ratio in the range 0.2 to 0.7. The maximum normalized electron collection efficiency is 0.81 and also occurs at 0.3, whereas for holes it ranges from 0.88 to 0.99. The most striking feature of figure 4(b) is that the electron collection efficiency in the top cell is significantly lower than it is for holes over the range of p-ratios studied. This is a direct result of surface recombination loss in the window layer, for which the surface recombination velocity (SRV) is $10^6cm\ sec^{-1}$. It will be shown that the electron collection efficiency increases significantly when SRV = 0. Moreover, the electron diffusion length in the window layer is 0.6 μm and in consideration of the window layer thickness being 0.1 μm, bulk recombination is negligible. Thus, we conclude that for SRV = $10^6cm\ sec^{-1}$ the surface recombination loss may be the major loss factor in the cascade cells studied.

It is instructive to compare the normalized collection efficiencies of this study with that reported for the AlGaAs-GaInAs [ref. 4]. In the latter, the collection efficiency exceeds 0.91 over the p-ratio range 0.1 to 0.9. The bandgap at the window surface is 1.80 eV which is a direct transition alloy and where the electron mobility is high. In figure 1 the window surface bandgap is 2.09 eV, which is an indirect transition alloy for which the mobility is significantly lower than it is for 1.80 eV in the model used in these studies. In both studies the window layer thickness is the same and the difference in photon absorption cannot completely explain the lower electron collection efficiency in Figures 4(b) and 5(b). Therefore, we conclude that the lower mobility in the AlGaAs-GaAs cascade cell window layer is partially responsible for the low electron collection efficiency and lower conversion efficiency.

Figure 4(c) shows the dependency of the electron and hole dark current coefficients on the p-ratio. The energy barriers located at X_1 and X_3 serve to form a "Potential Well" solar cell of the top cell [ref. 1-5]. Electrons are confined in Region 2 and holes in Region 3, producing electron and hole accumulation in their respective regions. This results in a further shift in the quasi-Fermi levels in each region in a direction which reduces dark current. Electron contribution to dark current increases as the p-region widens as shown in figure 4(c). Similarly, the hole contribution to dark current increases as the n-region widens (i.e., p-ratio decreases). The cascade photovoltage is a maximum in the p-ratio range 0.3 to 0.6, decreasing sharply outside this range.

Maximum power of the top junction, P_{mpT}, available to the cascade cell is 22.75 mW/cm^2, occurring at 0.4 as shown in figure 4(d). P_{mpT} follows the general behavior of the normalized electron collection efficiency. The electron collection efficiency is the stronger influence on P_{mpT} than the hole efficiency because a substantially higher photoexcited carrier concentration is produced on the p-side of the top junction than on the n-side.

The power utilization ratio is constant at 0.98 up to the p-ratio equal to 0.5 as is shown in figure 4(d). Decreasing at a slow rate for p-ratios greater than 0.5, it does not exhibit a strong function of this ratio. This results because the p-ratio, when normalized to the optimum value of X_3-X_1, cannot greatly affect the current mismatch between top and bottom cells.

Imposed on the curves calculated in figure 5 is the optimum p-ratio equal to 0.3, where the ratio $(X_3-X_1)/1.46$ is allowed to vary from 0.5 to 2.0. Maximum conversion efficiency is 27.6% in figure 5(a) and it occurs at 1.0 for the ratio. Therefore, the optimum thickness of the p-region is 0.44 μm while it is 1.02 μm for the n-region, where the sum is 1.46 μm. Ratios less than 1.0 show the conversion efficiency curve to have a large positive slope, resulting from decreases in the incomplete absorption loss in the top cell with increasing total thickness. The slope is more gradual and negative for ratios greater than 1.0, which is a result of less effective carrier confinement as Regions 2 and 3 widen with increasing $(X_3-X_1)/1.46$. This gives increased dark current and greater minority carrier recombination in the top cell.

The normalized collection efficiencies for electrons and holes are presented in figure 5(b). While the electron collection efficiency is relatively constant, the hole collection efficiency is decreasing sharply at a relatively constant rate over the ratio range 0.5 to 2.0. The behavior is obtained because of the relative values of the electron and hole diffusion lengths and the corresponding optimum p- and n-region thicknesses. The electron diffusion length is 1.5 times longer than the hole diffusion length, but at the same time the optimum p-region is less one-third the sum of the p- and n-region thicknesses. Thus, with increasing values of $(X_3-X_1)/1.46$, the ratio $(X_2-X_1)/L_n$ is less than unity, while the ratio $(X_3-X_2)/L_p$ exceeds unity in the range 1.5 to 2.0.

Excess current for top and bottom cells are shown in figure 5(c), where the affects of incomplete absorption loss decreases and recombination increases in the top cell with increasing values of $(X_3-X_1)/1.46$. In the range $(X_3-X_1)/1.46 < 1$ incomplete absorption loss is greater than the recombination loss, but in the range $(X_3-X_1)/1.46 > 1$ the opposite is true. Incomplete absorption serves to significantly increase ΔJ_{exB}, while producing only small changes in ΔJ_{exT}. Similarly, recombination loss produces a change in ΔJ_{exT}, while ΔJ_{exB} is nearly constant, in the range $(X_3-X_1)/1.46 > 1$.

For reasons similar to those discussed above, in figure 5(d) the maximum power of the top cell, P_{mpT}, and the power utilization ratio increase significantly with decreasing incomplete absorption loss, but they are nearly constant in the range where recombination loss dominates. Maximum power of the bottom cell, P_{mpB}, decreases with increasing $(X_3-X_1)/1.46$, because photon absorption in the top cell increases which results in a smaller photon flux available to the bottom cell. An asymptotic value is achieved when the top cell absorbs all of the photons with energy equal to or greater than 1.94 eV.

Figure 6 shows some of the effects produced by changes in the donor impurity concentration of Region 7 in the range $1 \times 10^{16}cm^{-3}$ to $3.2 \times 10^{18}cm^{-3}$. They correspond to the set of curves in figure 3, which show the effect on the top cell parameters arising from changes in the donor concentration in Region 3. There are striking similarities between the two sets of curves. The optimum donor concentration is $7 \times 10^{17}cm^{-3}$ for which the efficiency is 27.6% as shown in figure 6(a). The slope of the efficiency curve is not as steep for higher concentration values as is shown in figure 3(a). This results because the bottom cell makes a smaller contribution to the total cascade efficiency than does the top cell. Therefore, any change arising from the bottom cell affects the efficiency less than corresponding changes in the top cell. The top cell contributes 60% and the bottom cell 40% of the cascade cell efficiency.

The normalized collection efficiency and lifetime of holes in the bottom cell, shown in figure 6 (b), exhibit a behavior corresponding to those in figure 3(b) and produce similar results in the maximum power of the bottom cell as was produced in the top cell. Moreover, the power utilization ratio, maximum power point voltage of the bottom cell V-I curve, and the dark current components shown in figures 6(c) and 6(d) all exhibit a similar relationship as those shown in figure 3(c) and 3(d), respectively.

Corresponding ratios are defined for the bottom cell in the determination of optimum layer thicknesses as were used in the top cell optimization. The bottom cell p-ratio is defined by $(X_6-X_5)/3.25$ and the total thickness ratio is $(X_7-X_5)/3.25$, where it is shown subsequently that the optimum total thickness of the bottom cell is 3.25 μm.

Figures 7 and 8 exhibit the computer modeling results related to the bottom cell, and correspond to figures 4 and 5, respectively, of the top cell. While there are similarities between the corresponding curves in the figures, the

differences are more significant in comprehending the device physics of cascade cells.

Figure 7(a) shows maximum conversion efficiency to occur at a p-ratio of 0.4, whereas it occurs at 0.3 for the top cell. Comparing the curves in figures 7(b) and 4(b) shows that the bottom cell normalized electron collection efficiency appears to show greater sensitivity to the p-ratio of the bottom cell than the corresponding curves of the top cell. This is attributed to the absence of a loss in the bottom cell corresponding to the surface recombination loss, higher recombination loss in the bottom cell, and a less effective "Potential Well" in Region 7. These factors also give rise to the electron normalized collection efficiency being higher than for holes in the bottom cell which is exhibited in figure 7(b), whereas the opposite is true for the top cell as is evident in figure 4(b).

The curves in figures 7(c) and 4(c) behave similarly with the exception that the electron and hole dark current scale of the bottom cell is eight decades higher. This is due to the higher dark current in the bottom cell produced by its smaller bandgap value. The power utilization ratio and the respective maximum power in figures 7(d) and 4(d) also show similar behavior.

Conversion efficiency is relatively constant over the range 0.6 to 1.7 of the normalized total thickness as shown in figure 8(a), because the electron and hole normalized collection efficiencies, presented in figure 8(b), are not strong functions of the total thickness ratio in this range. In contrast, the top cell hole collection efficiency, figure 4(b), shows a strong dependency on the top cell total thickness ratio. This also results in a smaller change in ΔJ_{exT} and ΔJ_{exB} in figure 8(c) compared to the curves in figure 4(c). Similarly, the changes occurring in P_u and P_{mpB} in figure 8(d) are somewhat smaller than they are in figure 4(d). The value of P_{mpT} is constant because changes in the bottom cell cannot affect the top cell V-I curve.

Surface Recombination Loss

Studying the device performance characteristics presented in the above discussion, it is concluded that surface recombination in the window layer produces the biggest loss in the cascade cell model used above. Electron collection efficiency of the top cell, given in Figures 4(b) and 5(b), is significantly lower than either the hole collection efficiency of the top cell or the electron collection efficiency of the bottom cell. Although the hole collection efficiency of the bottom cell is less than 0.8, it makes a smaller contribution to the overall efficiency than do the photoelectrons generated in the top cell.

To illustrate the significance of the surface recombination loss, figure 9 shows the conversion efficiency vs the top cell bandgap, with surface recombination velocity a parameter. Each curve in figure 9 exhibits a pronounced maximum, at which the optimum bandgap value is obtained. The maximum efficiency value of each curve and its corresponding optimum bandgap increase with decreasing SRV. Decreasing SRV makes more photocurrent available to the top

cell and this results in an increase in $|\Delta J_{exT}|$. By increasing E_{GT}, $|\Delta J_{exT}|$ and the current mismatch between top and bottom cells are reduced which produces an increase in efficiency.

The structure used is that of the optimized design, including the window layer. While the serial optimization procedure was not used to obtain the results given in figure 9, at each of the maximum efficiency points the excess current and current mismatch between cells are characteristic of an optimized design.

Figure 9 shows that the efficiency may exceed 29% for SRV values less than 10^5cm sec^{-1}. The rate of decrease of efficiency in the SRV range 0 to 10^5cm sec^{-1} is considerably less than the rate above 10^5cm sec^{-1}. These results suggest that there may be merit in considering a substitute of the AlGaAs window used in our model.

Alternative structures are deserving of consideration to affect a reduction of the surface recombination loss. An obvious structure is to replace the window layer with a wide bandgap transparent layer which results in an interfacial recombination velocity less than 10^5cm sec.

The desirable window material characteristics are for lattice matching to p-AlGaAs, the direct and indirect bandgap energies are to be sufficiently high so that the photon absorption in the window layer is small compared to the absorption in the top cell, and for the interfacial recombination velocity to be less than 10^5cm sec^{-1}. In figure 1 this requires a material for which its bandgap energy exceeds 2.3 eV which cannot be achieved using the AlGaAs ternary. One candidate is ZnSe, which is under investigation for use in single junction n/p GaAs solar cells [ref. 14]. The lattice mismatch with GaAs is 0.3% for 2.6 eV bandgap ZnSe. In this work, it is reported that electron-hole recombination is reduced near the interface using an n-ZnSe window [ref. 14]. It is not clear from this work that interfacial recombination is also reduced using a p-ZnSe window on p-AlGaAs.

SUMMARY AND CONCLUSIONS

Computer modeling studies of the AlGaAs-GaAs, two-junction, cascade solar cell are reported suggesting that the upper limit on conversion efficiency is approximately 27%. A study of the device performance characteristics obtained shows that the surface recombination is responsible for the major loss in the theoretical device design which evolves. This results because the bandgap energy of the AlGaAs window layer is too small to serve as an effective window. Values of surface recombination velocity less than 10^5cm sec^{-1} result in an increase in the upper limit of efficiency to approximately 29%. For the AlGaAs-GaAs cascade cell to be an attractive alternative to other material combinations, it is recommended that effort be directed to reducing the surface recombination loss. There are a number of approaches for reducing the surface loss, however, it is not clear at this time which is the most promising or if the problem is solvable.

ACKNOWLEDGEMENTS

Discussions with J. A. Hutchby and S. Bedair were helpful in determining the limits imposed on the device parameters due to technology. We also acknowledge the suggestion by P. Rahilly of using ZnSe for the window material.

REFERENCES

1. Lamorte, M. F. and Abbott, D. H.: 12th IEEE Photovoltaic Specialists Conf., Baton Rouge, LA, Nov. 15-18, 1976.

2. Lamorte, M. F. and Abbott, D. H.: 13th IEEE Photovoltaic Specialists Conf., Washington, D.C., June 5-8, 1978.

3. Lamorte, M. F. and Abbott, D. H.: Solid-State Electronics 22, 467-73, 1979.

4. Lamorte, M. F. and Abbott, D. H.: IEEE Trans. Elect. Devices ED-27, 231-49, 1980.

5. Lamorte, M. F. and Abbott, D. H.: IEEE Trans. Elect. Devices ED-27, 831-40, 1980.

6. Bedair, S. M.; Lamorte, M. F. and Hauser, J. R.: Appl. Phys. Lett. 34, 38-39, 1979.

7. Bedair, S. M.; Lamorte, M. F.; Hauser, J. R.; and Mitchell, K. W.: IEEE International Elect. Devices Mtg., Washington, D. C., Dec. 5, 1978.

8. Casey, H. C., Jr.; and Panish, M. B.: Heterostructure Lasers Part A: Fundamental Principles, Academic Press, New York, 1978.

9. Hovel, H. J.: Solar Cells; Semiconductors and Semimetals, Vol. 11; Ed. R. K. Willardson and A. C. Beer, Academic Press, New York, 1975.

10. Bedair, S. M.: J. Appl. Phys. 50, 7267-68, 1979.

11. Bedair, S. M.: J. Appl. Phys. 51, 3935-37, 1980.

12. Bedair, S. M.: private communication.

13. Sze, S. M.: Physics of Semiconductor Devices, New York, Wiley, 1969.

14. Walsh, D. and Shing, Y. H., 14th IEEE Photovoltaic Specialists Conf.,

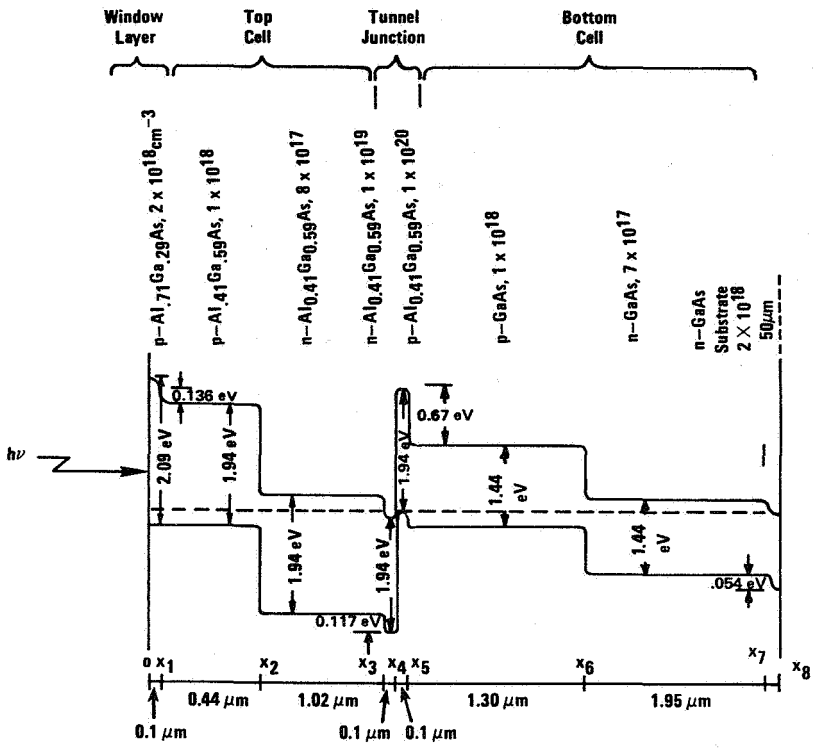

Figure 1. Bandstructure used in the study and parameters obtained for optimized design by maximizing conversion efficiency.

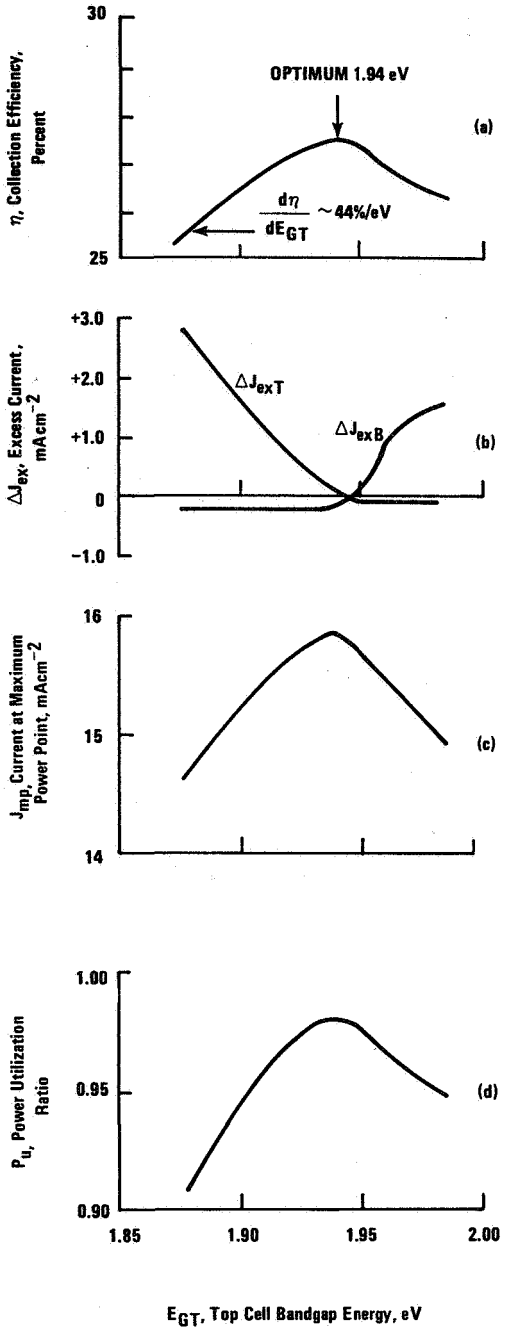

Figure 2. Determination of optimum top cell bandgap, E_{GT}: (a) conversion efficiency, (b) excess current, (c) current at maximum power point on cascade cell V-I curve, and (d) power utilization ratio; vs. E_{GT}.

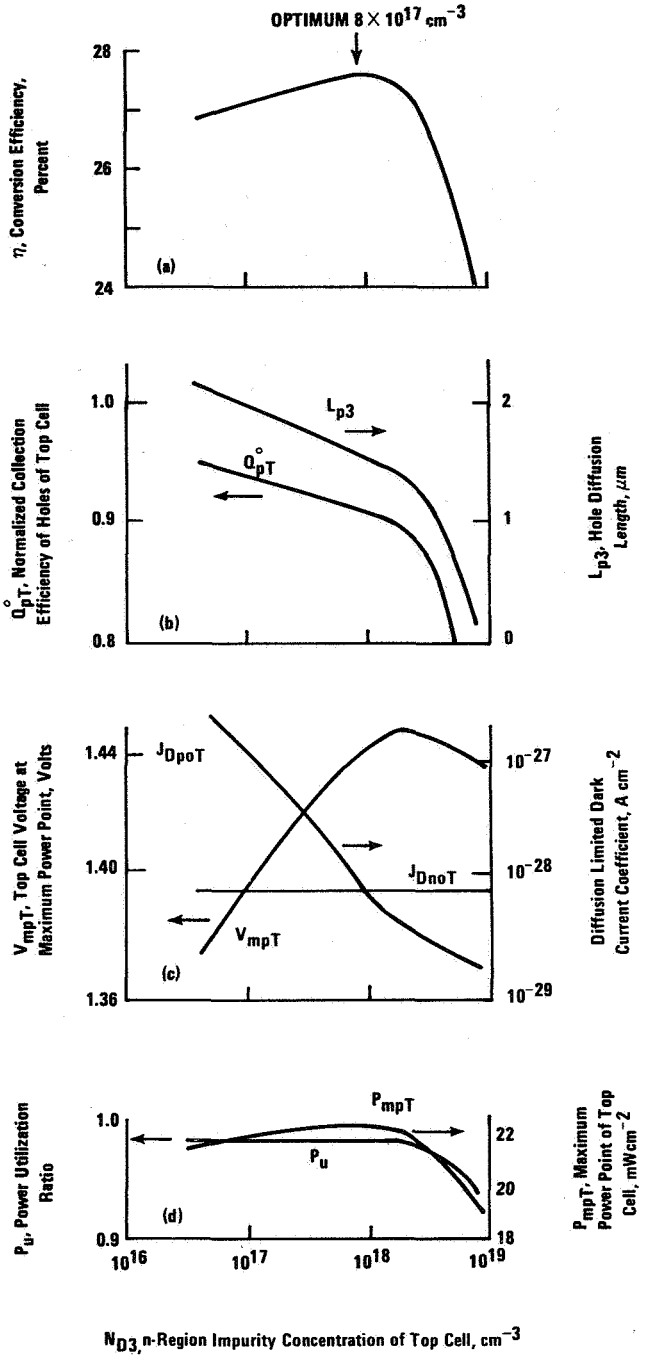

Figure 3. Determination of optimum donor concentration in Region 3, N_{D3}: (a) conversion efficiency, (b) normalized collection efficiency and diffusion length of holes, (c) voltage at maximum power point of top cell V-I curve and diffusion limited dark current coefficients, and (d) power utilization ratio and the maximum power point of top cell V-I curve; vs. N_{D3}.

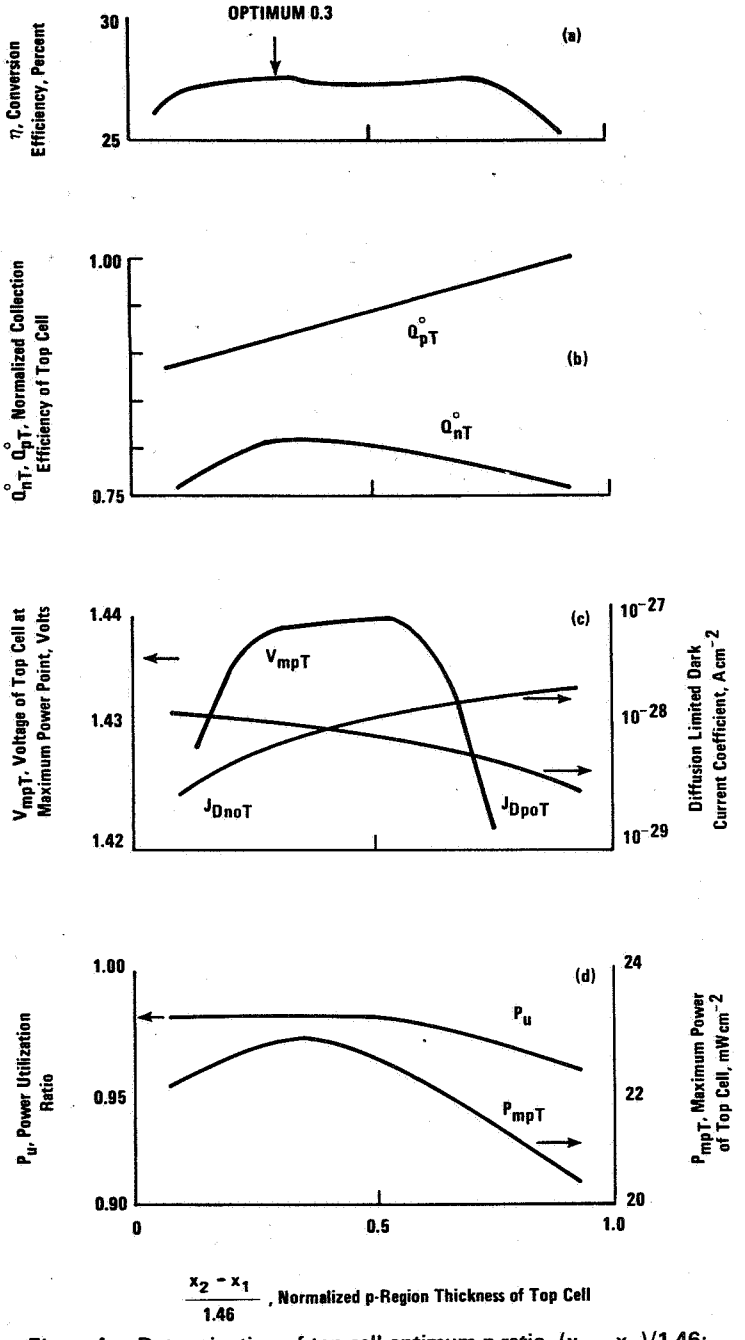

Figure 4. Determination of top cell optimum p-ratio, $(x_2 - x_1)/1.46$: (a) conversion efficiency, (b) normalized collection efficiencies (c) voltage at maximum power point of top cell V-I curve and diffusion limited dark current coefficients, and (d) power utilization ratio and maximum power point of top cell V-I curve; vs. $(x_2 - x_1)/1.46$.

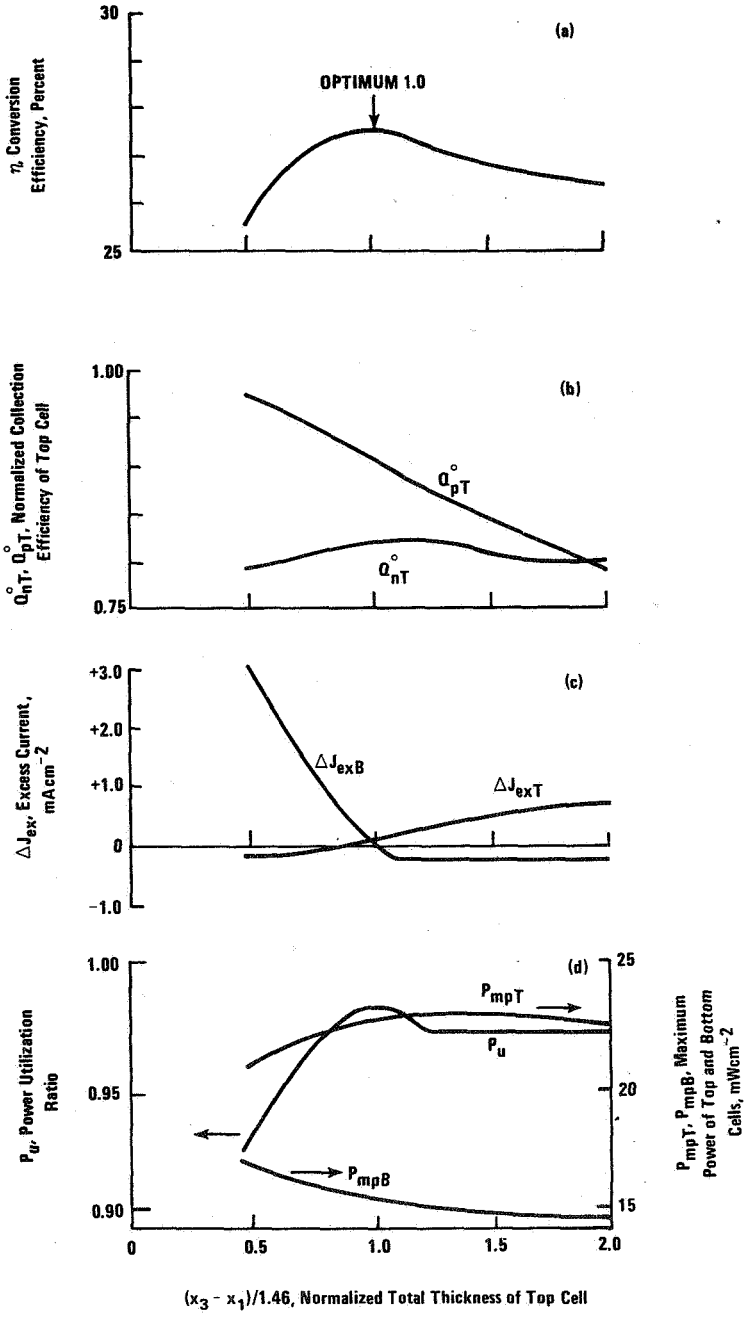

Figure 5. Determination of top cell optimum total thickness ratio, $(x_3 - x_1)/1.46$: (a) conversion efficiency, (b) normalized collection efficiencies, (c) excess currents of top and bottom cells, and (d) power utilization ratio and maximum power points of the top and bottom cell V-I curves; vs. $(x_3 - x_1)/1.46$.

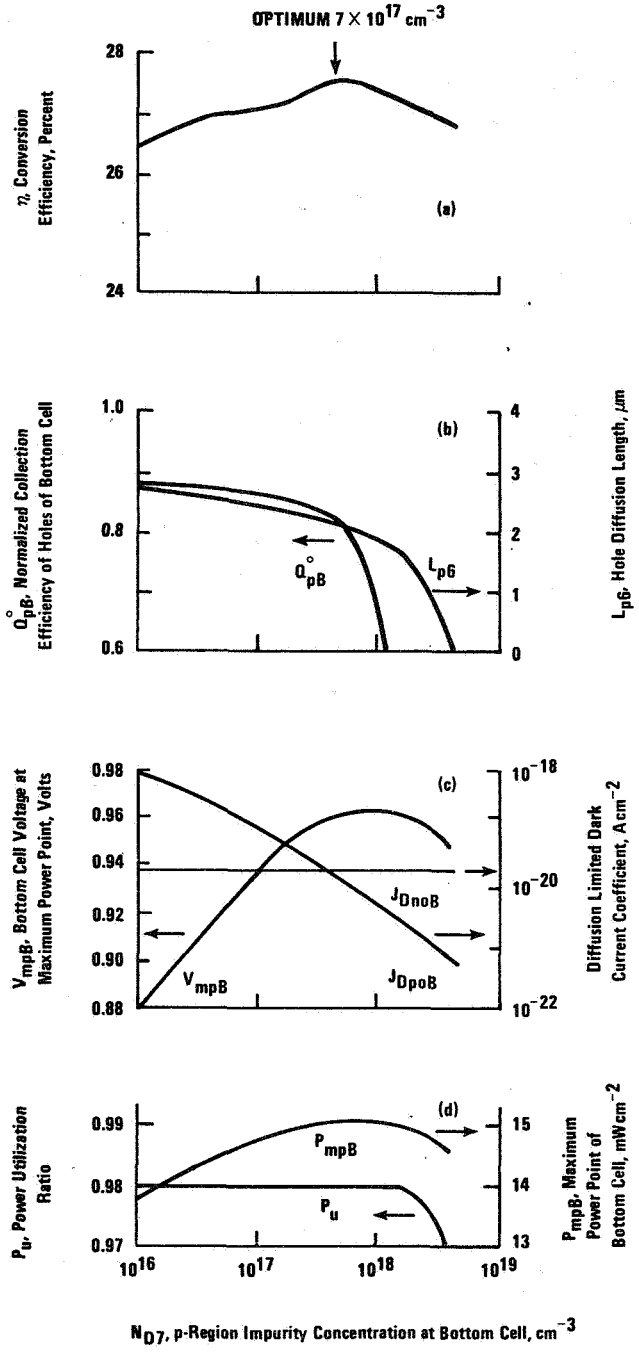

Figure 6. Determination of optimum donor concentration in Region 7, N_{D7}: (a) conversion efficiency, (b) normalized collection efficiency and diffusion length of holes, (c) voltage at maximum power point of bottom cell V-I curve and diffusion limited dark current coefficients, and (d) power utilization ratio and maximum power point of bottom cell V-I curve; vs. N_{D7}.

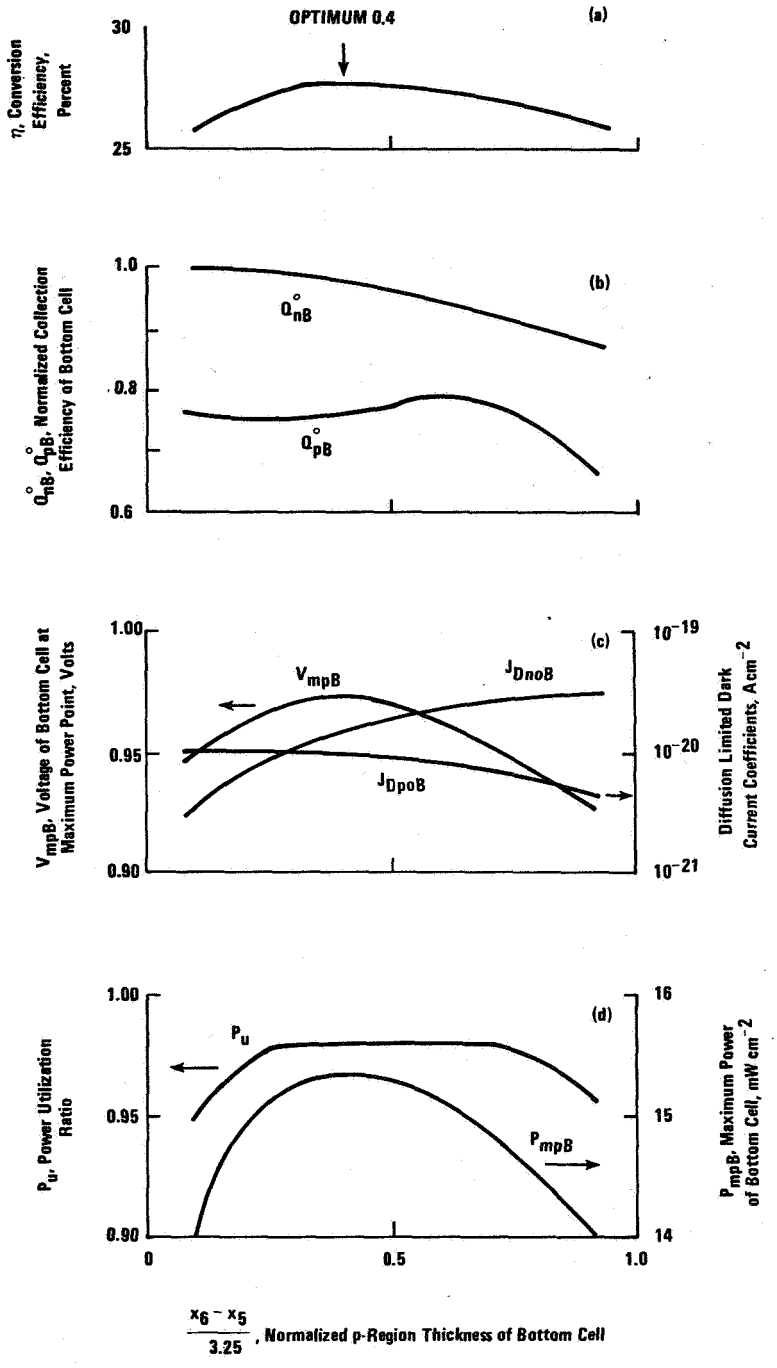

Figure 7. Determination of optimum p-ratio, $(x_6 - x_5)/3.25$: (a) conversion efficiency, (b) normalized collection efficiencies, (c) voltage at the maximum power point of bottom cell V-I curve and diffusion limited dark current coefficients, and (d) power utilization ratio and maximum power point of bottom cell V-I curve; $(x_6 - x_5)/3.25$.

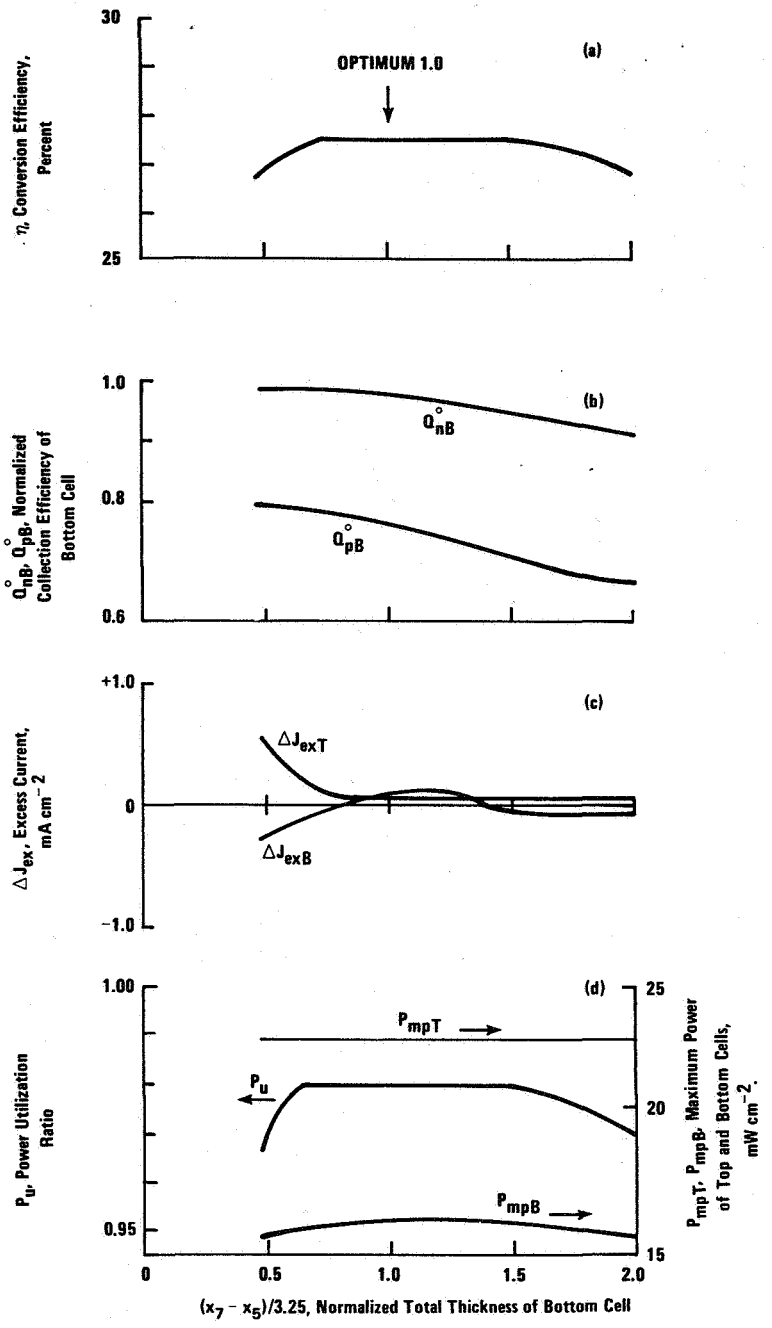

Figure 8. Determination of bottom cell optimum total thickness ratio, $(x_7 - x_5)/3.25$: (a) conversion efficiency, (b) normalized collection efficiencies, (c) excess currents, and (d) power utilization ratio and maximum power points on top and bottom cell V-I curves; vs. $(x_7 - x_5)/3.25$.

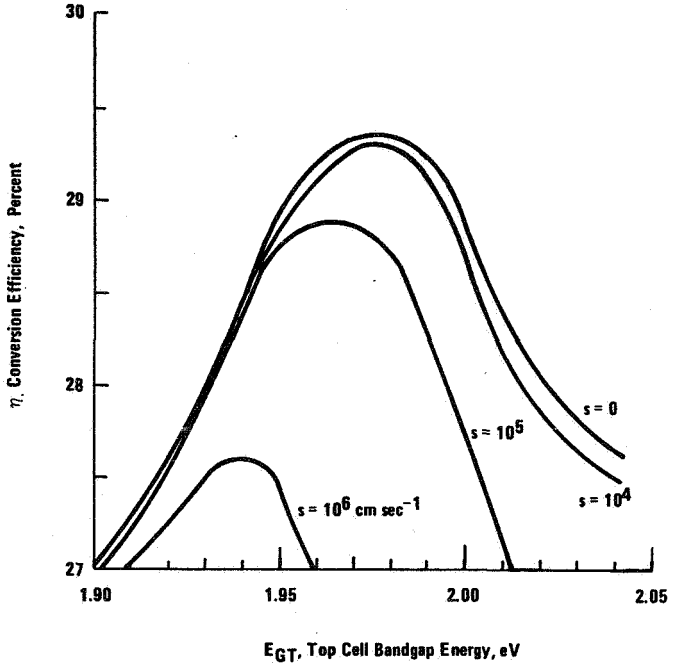

Figure 9. Conversion efficiency vs. top cell bandgap with surface recombination velocity as a parameter.